OFDM Radar Range Accuracy Enhancement Using Fractional Fourier Transformation and Phase Analysis Techniques

Jianguo Li, Sining An, Jianping An, *Member, IEEE*,
Herbert Zirath, *Fellow Member, IEEE* and Zhongxia Simon He *Member, IEEE*

***Abstract*—Orthogonal Frequency Division Multiplexing (OFDM) technique is obtained significant attention in radar applications for its interference resilience property. In this paper, Fractional Fourier Transformation (FRFT) and phase analysis techniques are proposed to enhance ranging accuracy of an OFDM Radar. A proof-of-concept radar is built and tested at 79 GHz and a range accuracy of 20 μm at 5 MHz measurement rate was measured. The range accuracy is 500 times higher compared with the application of fast Fourier transformation (FFT) method.**

***Index Terms*—OFDM Radar, Phase Analysis Technique, Fractional Fourier Transformation, Range accuracy**

I. Introduction

THERE are two hot topics within information technology area nowadays, one is Industrial 4.0, another is the fifth generation of mobile network (5G). Industrial 4.0 was proposed in 2011 focusing on connecting all machines with robotics in the factory to form an agile, reconfigurable factory which can be used to produce diverse commodity base on demand [1]. Besides, 5G mobile infrastructure promises high data rate, low latency and higher quality of service [2], [3],which, undoubtedly, will accelerate the development of the future smart factory through providing massive low latency wireless connections which can bring factory monitoring and control to a new level. Moveover, sensors play a crucial role in realizing a fully configurable robotic tools in the future factory. In addition to robotic motion monitoring, it is also important to monitoring human workers to avoid robotic arm and worker collision. A 5G C-band radar was demonstrated for human motion detection in [4], [5]. Moreover, high-precision sensors play a decisive role in the production of sophisticated equipment such as robotic arms, CNC lathes, milling machines, etc.

Past decades have witnessed the application of various sensors, such as accelerometer, temperature/humidity meter, laser and ultrasound sensor in factories. [6], [7]. Definitely, robotic arms will play prominent roles in advanced automation [8]. One critical issue is to prevent these robotic arms from colliding into each other, as well as to ensure that the robotic arm can manipulate objects with ultra-high accuracy. To measure the distance between robotic arms and that between the arm and the object under manufacturing, several sensors are used including laser, ultrasonic and radar [9]. Laser requires a clear view of the target which is not viable in some applications. While ultrasonic sensors are relatively of low cost, but it is hard to avoid interference when multiple sensors are closely installed. A radar system of high distance accuracy and interference resilience is of great interest for high-precision robotic arm manipulation and to avoid collision between robotic arms.

TABLE I: Demographic Prediction performance comparison by three evaluation metrics.

Ref.	Freq. (GHz)	Bandwidth	Method	Accuracy (μm)	Unambiguous Range	Measurement Rate
[10]	80	2 GHz	FMCW	± 8	≥5 m	0.25 kHz
[11]	121	6 GHz	FMCW	± 6	≥ 1km	62.77 Hz
[12]	122.5	1 GHz	FMCW	± 2	≥1 km	1 kHz
[13]	80	10 GHz	FMCW	± 0.5	≥1 km	250 Hz
[14]	24	50 kHz	Interferometer	± 0.5	≥1.25 cm	≤10 kHz
[15]	24	250 MHz	2-tone Interferometer	± 35	≥48.4 cm	≤10 kHz
This	79	2 GHz	OFDM and FRFT	± 20	≥1 km	5 MHz

Various radar systems were adopted for high-precision applications with their performance summarized in Table. I. In the literature [10], an unambiguous phase-based FMCW radar algorithm for micron accuracy distance measurements was proposed. The unambiguous single measurement accuracy has been improved from about 400 μm to 8 μm at 80 GHz. The authors in [11] have proposed a highly miniaturized and commercially available millimeter wave radar sensor working in the 121-127 GHz, which can be utilized for micrometer range accuracy. FMCW radars at 120 GHz band have achieved micrometer level range accuracy [12], [13], but the measurement rate is often limited by the frequency sweep speed. Interferometer techniques with single tone or dual tone can be used to measure targets at high rate, but range ambiguity appears when target moves out of a limited range window

This work was partially funded by National Nature Science Foundation of China (61620106001) and the car2TERA project which has received funding from the European Union's Horizon 2020 research and innovation programme under grant agreement NO 824962.

J. Li, J. An are with the Beijing Institute of Technology, Beijing, China. S. An, Z. He (zhongxia@chalmers.se) and H. Zirath are with Chalmers University of Technology, Göteborg, Sweden

[14], [15]. Due to the high frequency and short wavelength of the millimeter wave, ultra-high ranging accuracy can be achieved by determining the carrier phase, and OFDM can resist interference by means of code division. Therefore, the millimeter wave OFDM radar sensor achieves high-precision measurement under strong interference.

Orthogonal Frequency Division Multiplexing radar waveform has been proposed in [16], which can perform radar detection as well as communication simultaneously. Based on the application of diverse signature codes to each sensor, multiple radars can operate simultaneously free of interference. When applying FFT, the range accuracy and resolution OFDM radar are inversely proportional to the bandwidth B of the transmitted signal, as $\delta R = c_0/2B$, where c_0 is the speed of light.

OFDM radar, with its multi-carrier parallel transmission and reception characteristics, has attracted wide attention in high-precision rang. Random OFDM pair radar based on compressive sensing with high resolution range reconstruction was proposed in [17], [18]. Meanwhile, the adaptive OFDM radar waveform design methods were proposed for improved micro-doppler estimation in [19], [20]. Then, the authors in [21] has proposed a OFDM integrated radar and communications waveform design method to improve the effectiveness of limited spectral resources. In addition, a two-step doppler estimation scheme was introduced in [22]. Moreover, a novel signal processing approach for OFDM radar has been presented in [23], which can overcome the effects of doppler in OFDM. Furthermore, a high accuracy doppler processing method for the OFDM radar and communication system has been introduced in [24].

In this paper, we proposed an OFDM radar accuracy enhancement technique , which, compared to traditional FFT estimation result, provides 500-times accuracy improvement . With a bandwidth of B = 2 GHz, the distance measurement of a metal target has an error less than 20 μm. Such result is experimentally verified using an OFDM radar operating at 80 GHz. This paper is organized as following: The introduction is given in section I. In section II, the OFDM radar operation principle is reviewed and the enhancement techniques are introduced. The implementation detail of the proposed OFDM radar is given in section III. Interference from other radar is studied and the result is discussed in section IV. A laboratory experimental setup is illustrated and the measurement result is presented in section V. Conclusion and summary is presented in section VI.

II. REVIEW OFDM RADAR CONCEPT AND RANGE ACCURACY LIMITATION

The operational principle of an OFDM radar has been discussed in detail in [16]. An OFDM multicarrier signal can be denoted as a composite of multiple parallel orthogonal signal carrier signals which modulated with different transmission data. And the transmission data can be written as:

$$x(t) = \sum_{\mu=0}^{N_{sym}-1} \sum_{n=0}^{N_c-1} a(\mu N_c+n)\exp(j2\pi f_n t)\mathrm{rect}(\frac{t-\mu T_{OFDM}}{T_{OFDM}}), \quad (1)$$

where μ is the OFDM symbol index within the total amount of N_{sym} OFDM symbols, n is the subcarrier index with in the total amount of N_c subcarriers, a is the complex modulation symbol, f_n is the subcarrier frequency and T_{OFDM} is the OFDM symbol duration.

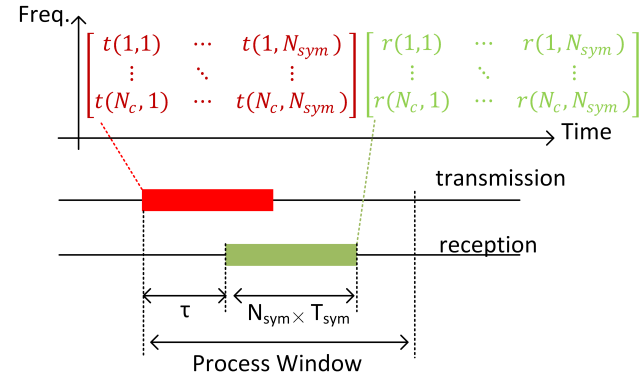

(a) time domain waveform of transmitted and received radar signal.

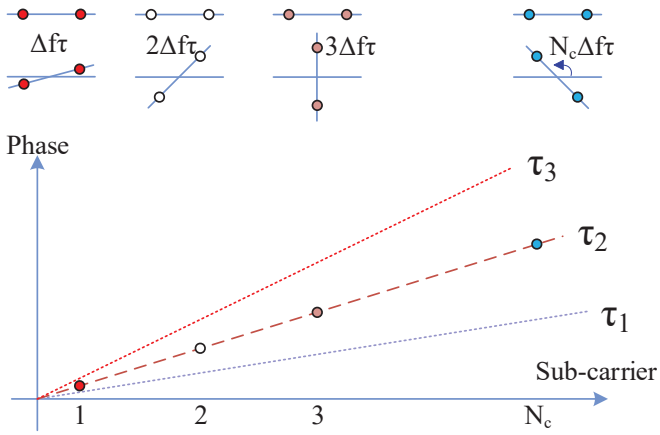

(b) illustration of the phase rotation at each subcarrier.

Fig. 1: The intuitive explanation of OFDM radar.

In this paragraph, we introduce an intuitive explanation that illustrated in Fig. 1 as complimentary to the equations expressions in [16]. Assuming a transmission waveform comprises N_{sym} symbols of each symbol duration of T_{sym}, each of the symbol is a sum of N_c subcarriers with subcarrier spacing of $\Delta f = 1/T_{sym}$. The initial phase of each subcarrier at each symbol is defined in the red matrix as shown in Fig. 1(a). Here we define a matrix:

$$T = \begin{bmatrix} t(1,1) & \cdots & t(1,N_{sym}) \\ \vdots & \ddots & \vdots \\ t(N_c,1) & \cdots & t(N_c,N_{sym}) \end{bmatrix}. \quad (2)$$

Each element in matrix T is a complex number to represent the phase of transmission, the first index denotes the subcarrier number and the second index denotes the symbol number. The red waveform in Fig. 1(a) contains $N_c \times N_{sym}$ symbols, for each transmitter the matrix T is fixed as a signature code. In this work, BPSK modulation is used,

therefore $t(m,n) \in [0,\pi]$. The receiver is fully synchronized with the transmitter, the echo reflected from a target would generate a green waveform which is delayed τ as shown in Fig. 1(a). The method of estimating this delay with high accuracy will be the focus of this paper. With an observation window that is designed wide enough, it allows the reception echo to be captured completely. Since the receiver is fully synchronized with the transmitter, the received signal matrix can be constructed similar as Eq. 2, the received signal matrix R can be written as:

$$R = \begin{bmatrix} r(1,1) & \cdots & r(1,N_{sym}) \\ \vdots & \ddots & \vdots \\ r(N_c,1) & \cdots & r(N_c,N_{sym}) \end{bmatrix}. \tag{3}$$

Note that the received signal contains the delay information that is of our interest. By dividing matrix R with matrix T, the signal transmission channel can be modelled in both time and frequency domain using a matrix $D = R/T$. Such matrix was described as Eq. 16 in [16] which is rewritten here as:

$$D = \begin{bmatrix} d(1,1) & \cdots & d(1,N_{sym}) \\ \vdots & \ddots & \vdots \\ d(N_c,1) & \cdots & d(N_c,N_{sym}) \end{bmatrix}. \tag{4}$$

The matrix T and R are illustrated in Fig. 1(b) for more intuitive understanding. On the top of Fig. 1(b), four BPSK constellation diagrams are shown with different color, which are corresponding to subcarrier 1, subcarrier 2, subcarrier 3 and subcarrier N_c, respectively. For instance, the constellation diagram of subcarrier 1 corresponds to the first row of the matrix T. The constellation diagrams below are the received constellation for different subcarriers. Similarly, each constellation diagram corresponds to a certain row in matrix R. It can be noticed that when a single target is presented, the constellation at higher subcarriers is more rotated than those at lower subcarriers. The matrix D is the channel information as discussed before, each row in D represents the constellation rotation measurements at each subcarrier. Such measurements are made at the reception of every symbol, thus N_{sym} data in each row. Averaging can be made over each row thus matrix D converts into vector:

$$D' = \begin{bmatrix} \overline{d_1} \\ \overline{d_2} \\ \vdots \\ \overline{d_{N_c}} \end{bmatrix}, \tag{5}$$

where $\overline{d_m}$ is a complex number of the mean rotation of the constellation diagram at m-th subcarrier. Vector D' is plotted at the bottom of Fig. 1(b) with angle at the Y-axis and the frequencies of each subcarrier at the X-axis. As mentioned before with an ideal single target, the rotation angle increases linear as the subcarrier frequency increases, the rotation angle at k-th subcarrier can be written as:

$$\varphi_k = 2\pi \times (f_c + k \times \Delta f) \times \tau. \tag{6}$$

A range estimation method is proposed in [16] using IDFT operations:

$$\begin{aligned} r(k) = IDFT[D'] &= \frac{1}{N_c}\sum_{n=0}^{N_c-1} D'(n) exp(\frac{j2\pi}{N_c}nk) \\ &= \frac{1}{N_c}\sum_{n=0}^{N_c-1} exp(-j2\pi n\Delta f\tau) exp(\frac{j2\pi}{N_c}nk). \end{aligned} \tag{7}$$

It can be seen two exponential terms would cancel each other and result in unity when:

$$k = \lfloor \Delta f N_c \tau \rfloor, k = 0, ..., N_c - 1. \tag{8}$$

That means a peak would occur at index of k in the time response of $r(k)$ which indicate a target is detected at that position. The accuracy using such method is limited by the fact that IDFT is used. It can be seen the target range searching is made in a discrete step of $\delta R = \frac{C_0}{2N_c\Delta f}$.

This is illustrated in Fig. 1(b) as several dotted reference lines with different slope is used to compare with the observed rotation angles. Intuitively, if more reference lines are used with finer steps that would give more accurate estimation. A fractional Fourier transform based method is introduced in the following section to improve the estimation accuracy.

III. FRFT AND PHASE ANALYSIS TECHNIQUES

As mentioned above the accuracy of the range resolution is a result of using a conventional Fourier transform as shown in Eq. 7. In this paper we have proposed a two-step signal processing method that can improve range accuracy to micrometer level. The first-step is using FRFT instead of Fourier transform. The second-step uses the phase information of a carrier to further enhance estimation accuracy. Both steps are introduced and discussed in this section.

A. Range Accuracy Enhancement with FRFT

As mentioned in previous section, modifying the Eq. 7 by simply adding more searching steps will increase the estimation accuracy. By introducing a fractional factor ma, the estimation function using FRFT can be written as:

$$r(k) = \frac{1}{ma \times N_c}\sum_{n=0}^{ma\times N_c-1} exp(-j2\pi n\Delta f\tau) exp(\frac{j2\pi nk}{ma \times N_c}). \tag{9}$$

The fractional factor defines ma times points are searched whose results in a correlation curve as shown in Fig. 2. The figure shows the simulation result using FRFT method where the simulation scenario is: 128 subcarriers with spacing of 15.625 MHz, ma = 20, carrier frequency 80 GHz, target distance set at 240 mm and 243.75 mm.

When using Eq. 7, the target at these two position results in identical peaks are indicating that the estimation distance is 75 mm. Clearly, such small distance change cannot be tracked by the conventional method. By using FRFT method,

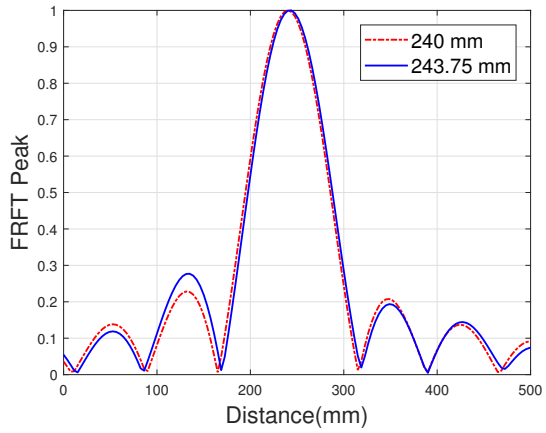

(a) simulated peak of target at different location.

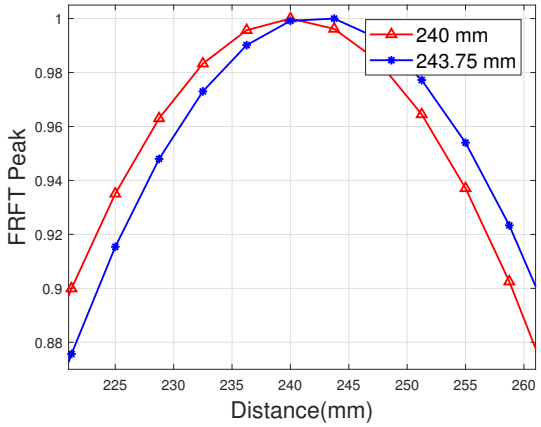

(b) zoom-in view of the correlation peak.

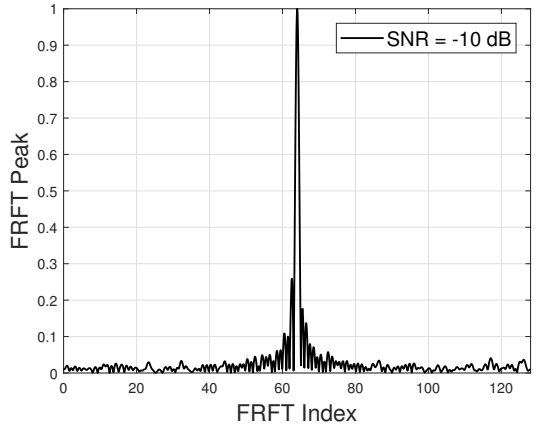

(c) simulated correlation peak at a low SNR after correlation with a "sinc" function.

Fig. 2: Simulated FRFT correlation peak when the target is at 240 mm and 243.75 mm.

the estimation curves are shown in Fig. 2(a), the red curve corresponds to the target at 240 mm position and the blue curve corresponds to the target at 243.75 mm. The zoomed in figure is shown in Fig. 2(b). It can be seen due to the fine accuracy of the estimation curve the target movement can be tracked with high confidence. Simulation is also performed at low SNR scenario (SNR = -10 dB), as expected, the correlation peak is not pronounced as the ideal case. To resolve this practical issue, the curves in Fig. 2(c) are correlated with ideal "sinc" function as expressed in the equation below, then the correlation peaks appear again after this process.

$$\begin{aligned} r(k) &= \frac{1}{ma \times N_c} \sum_{n=0}^{ma\times N_c-1} exp(-j2\pi n\Delta f\tau) exp(\frac{j2\pi nk}{ma \times N_c}) \\ &= \frac{1}{ma \times N_c} \sum_{n=0}^{ma\times N_c-1} exp(j2\pi n(\frac{k}{ma \times N_c} - \Delta f\tau)) \end{aligned}, \tag{10}$$

Where

$$\Delta\tau = \frac{k}{ma \times N_c} - \Delta f\tau, \tag{11}$$

Then the equation can be further simplified into

$$\begin{aligned} r(k) &= \frac{1}{ma \times N_c} \sum_{n=0}^{ma\times N_c-1} exp(j2\pi n\Delta\tau) \\ &= \frac{1}{ma \times N_c} \frac{1 - exp(j2\pi\Delta\tau \times ma \times N_c)}{1 - exp(j2\pi\Delta\tau)} \\ &= \frac{1}{ma \times N_c} \frac{sin(\pi\Delta\tau \times ma \times N_c)}{sin(\pi\Delta\tau)} \\ &\approx \frac{1}{ma \times N_c} \frac{sin(\pi\Delta\tau \times ma \times N_c)}{\pi\Delta\tau} \\ &= sinc(\Delta\tau \times ma \times N_c). \end{aligned} \tag{12}$$

The achievable range accuracy depends on several system parameters such as SNR, quadrature balance, in band flatness, etc. In our system, the correlation method is only used for coarse estimation. As long as the estimation accuracy is better than the wavelength of the carrier, the phase estimation can be used for further improvement of the accuracy down to micrometer level. The phase assisted estimation method is discussed in the following section.

B. Range Accuracy Enhancement with Phase Analysis

Taking the advantage of the short wavelength of the millimeter wave carrier, phase rotation occurs even with micrometers target displacement. By examining the phase of the modulated carrier, the distance of the target can be tracked with micrometer level accuracy. Such a method is widely used by interferometer radars [14], [15], however, ambiguity appears when the target moves more than one carrier wavelength.

In this paper, as we demonstrated in previous section, the proposed FRFT method can locate the target with accuracy less than half a wavelength. Adding phase analysis allows us further to improve the accuracy into micrometer level. The distance of the target can be written as follows:

$$R = m \times \lambda_c + R'. \tag{13}$$

For any subcarrier in the OFDM symbol, the target equals m-times carrier wavelength with a remained distance R'‘λ_c. The range estimation $\widehat{R}_{OFDM}$ obtained by the FRFT method above is used for calculating the integer number m. The

estimation error will be eliminated by a quantizing procedure. The remaining distance is calculated by:

$$R' = \frac{\phi}{2\pi} \times \lambda_c, \tag{14}$$

where ϕ is the received constellation rotation at the subcarrier of wavelength λ_c. At 80 GHz ($\lambda_c = 3.75mm$), for example, a 0.1° rotation equals to 1 µm target movement. The range estimation accuracy is then translated into angle resolution of the constellation rotation.

By using the proposed two-step method, the distance of the target can be estimated using Eq. 14 with wide unambiguous window. Experimental validation of this method is presented in the following section.

IV. MULTI-RADAR INTERFERENCE CANCELLATION

The proposed OFDM radar utilizes a signature code when sensing the target. With multiple signature codes, radars can be installed closely without interfering with each other. In this section the principle and performance benchmark are presented and analysis in a multiple radar coexisting scenario.

As mentioned above, the radar transmitting a specific symbol sequence as T, shown in Eq. 2. By assigning orthogonal symbol sequence to different radar, the interference between radars can be minimized. In our work, the selected transmitting symbol sequence is an m-sequence generated by polynomial $p(x) = x^7 + x^6 + 1$ using linear feedback shift register techniques. By assigning different M-sequence codes to different radars, radars can work simultaneously. To understand the performance of radar under interference, simulations are conducted for the situation that a radar is operated under the influence of another radar. The simulation result is presented in Fig. 3.

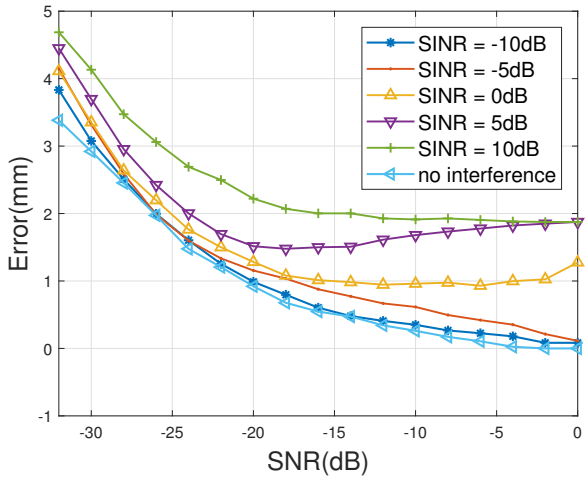

Fig. 3: Simulated range accuracy of OFDM radar under the influence of another radar operating in the same frequency band.

In this simulation, 128-bit M-sequences are assigned into two radars which operate at the same frequency. The target range error is plotted versus received SNR. Firstly when only one radar is operated, the estimation error is plotted as "no interference". Then another in-band operated radar is added with the signal-to-interference-plus-noise ratio (SINR) varying from -10 dB to 10 dB. The simulation results are as follows:

- The estimation error less than half of the carrier wavelength (79 GHz, 1.85 mm) can achieved even at -22 dB SNR with the SINR of 5 dB.
- Due to the fact that estimation is made by averaging 128 sub-carrier, the proposed radar is relatively immune to in-band interference. When the SINR = 10 dB, the Radar can also work well.
- The simulation shows that at SINR = 5 dB, estimation with half of the wavelength can still be achieved at SNR= -22 dB. It means that the range accurate can be further improved by phase analysis at SNR = -22 dB when the SINR = 5 dB.

V. EXPERIMENTAL RESULT

The proposed OFDM radar is experimentally verified using commercially available transceiver modules at 79 GHz in a laboratory environment. In this section, the experimental setup is introduced and measurement results are presented and discussed.

A. Experimental Setup

The photo of the laboratory experimental setup is shown in Fig. 4. Integrated E-band transmitter and receiver modules are used to generate and receive signal at 79 GHz.

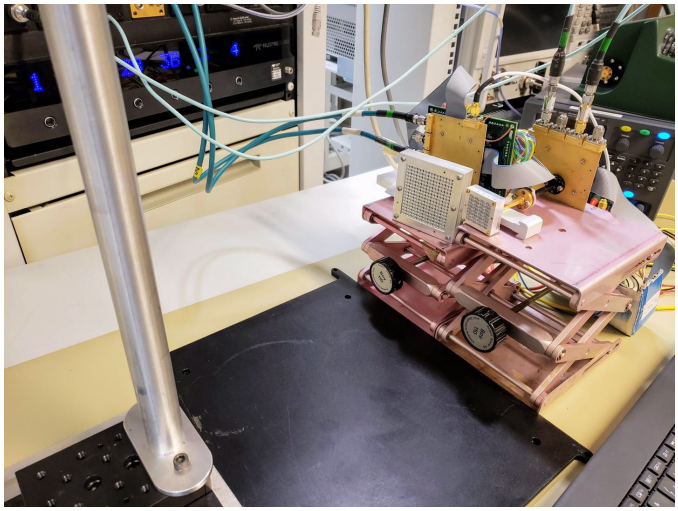

Fig. 4: Photo of the radar experiment setup in the lab.

Two planar E-band antennas are used, with separate antennas, more than 50 dB isolation between transceivers is achieved. A metal bar is used as a target which is located 24 cm away from the radar. An arbitrary waveform generator (AWG) is used to generate OFDM signal and a real-time oscilloscope is used to capture the received signal, the received data is processed off-line using Matlab.

In Fig. 5, the detailed diagram of the setup is depicted. In the AWG, the user code is used to generate a transmission matrix T as in Eq. 2. 128 subcarriers are used with channel spacing

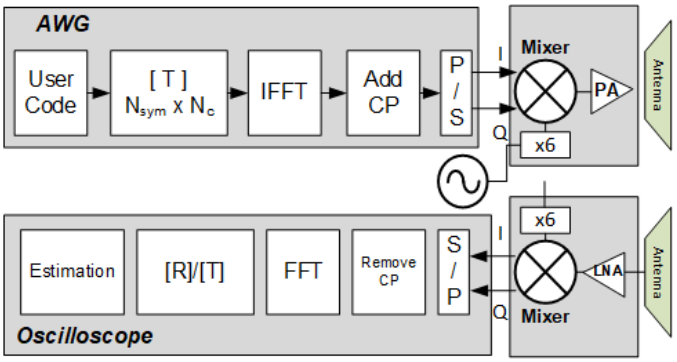

Fig. 5: Detailed diagram of the setup.

of 15.625 MHz, therefore a total bandwidth of 2 GHz is occupied. The time domain waveform is generated using 1024 points IFFT, and cyclic prefix (CP) is added. The waveform is then converted from parallel into serial (P/S) and output from AWG at 16 Gsps. An E-band transmitter (Gotmic gtsc0023) is used with 13 dBm averaged output power. A 30 dBi antenna is used at the transmitter side. A 25 dBi receiver antenna is used together with E-band receiver (Gotmic gRsc0013). Transmitter and receiver are sharing the same local oscillator (LO), therefore the phase between transmitter and receiver are fully synchronized. The received quadrature baseband signals are sampled by an oscilloscope.

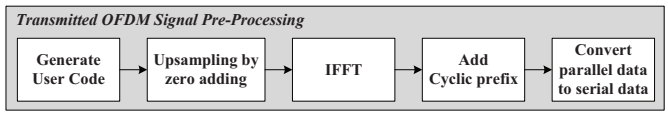

(a) The detailed transmitted pre-processing steps for OFDM radar.

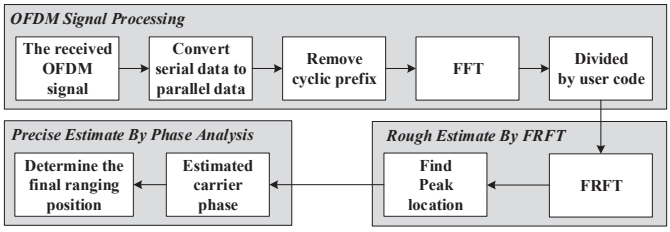

(b) The detailed received processing steps for OFDM radar.

Fig. 6: The detailed processing steps for OFDM radar.

The detailed transmitted pre-processing steps for OFDM radar are shown in Fig. 6(a). The user code was generated at first to distinguish each user. Then we did upsampling by zero adding. Next, IFFT was used to generate the OFDM signal. In addition, the cyclic prefix was added to resist multipath problems. Finally, we converted the parallel data to serial data. Moreover, the detailed received processing steps for OFDM radar are illustrated in Fig. 6(b). At the first stage, the OFDM signal should be processed. We convert serial data to parallel data, and then the cyclic prefix of OFDM signal is removed. Furthermore, the FFT can be used to demodulate the OFDM signal. Finally, the phase information can be uniquely left by dividing by the user codes. At the second stage, the peak location of the FRFT can be used to do rough estimate as mentioned in section III. At the last stage, since the estimation accuracy of the second stage is already within one wavelength, the phase analysis can be adopted to further improve the range accuracy.

B. Experimental Result

The normalized received signal spectrum is shown in Fig. 7. The signal occupies 2 GHz bandwidth with a received SNR higher than 20 dB. The received power is -17 dBm when the target is 240 mm away. Considering the path loss, the radar cross-section (RCS) is -38.4 dB/mm2.

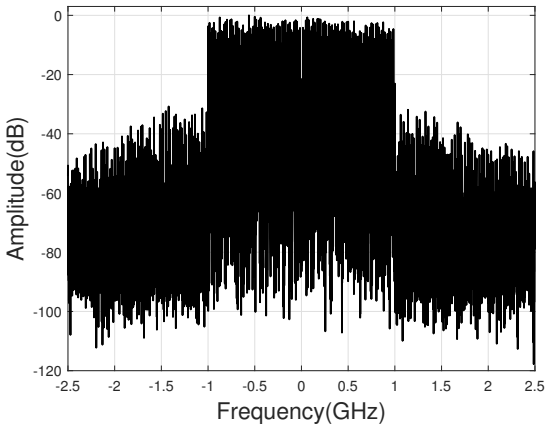

Fig. 7: The normalized received signal spectrum.

The target is then moved from 240 mm to 248 mm with 1 mm steps using a manual micrometer positioner. The measured phase of different subcarriers is plotted in Fig. 8 when target locates at 240 mm, 243 mm and 246 mm respectively.

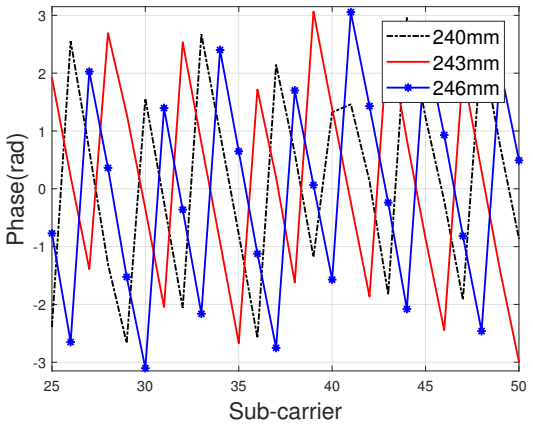

Fig. 8: The measured phase of different subcarriers.

As described in section II, the phase slope is changed proportional to the target distance as expected. Using FRFT method, the target distance can be estimated as it shown in Fig. 9. As long as the error of this estimation is less than the wavelength (3.7 mm), the distance can be further improved with phase analysis.

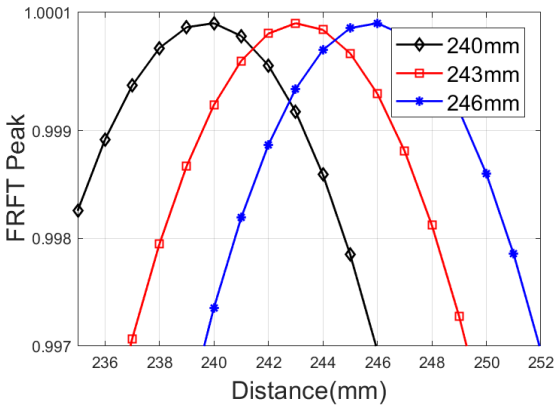

Fig. 9: The estimated target distance by FRFT method.

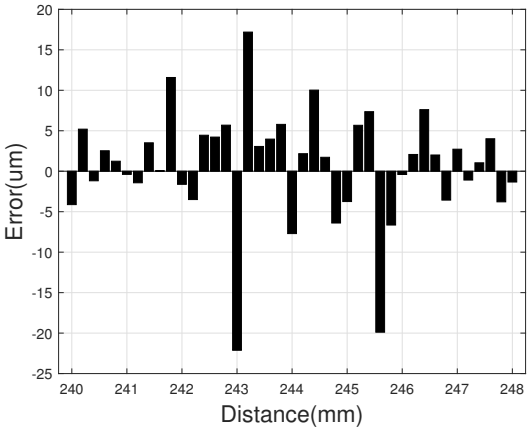

Fig. 10: The final estimated result by phase analysis method.

Adding phase analysis mentioned in section III. B, the final estimation result is presented in Fig. 10. It can be seen the error of the estimation is less than $\pm 20 \mu m$.

VI. Conclusion

An enhanced accuracy OFDM Radar is presented in this paper in which the FRFT and phase analysis techniques are adopted. FRFT is used to make the ranging accuracy of the target within one wavelength of the millimeter wave, followed by the utilization of the carrier phase analysis method to further improve the ranging accuracy, which can make the ranging accuracy of the target reach 20 μm.

Compared with the other published works summarized in Table. I, the proposed OFDM radar can achieve high accuracy at a high refresh rate over a long unambiguous range which mainly benefits from the parallel characteristics of OFDM and the short wavelength of millimeter wave. In the future work, we will adopt the higher frequency such as Terahertz band to further improve the range accuracy. In addition, multiple millimeter wave OFDM radar sensors can be utilized to multidimensional ranging for high-precision positioning and imaging.

Acknowledgment

This work was partially funded by National Nature Science Foundation of China (61620106001) and the car2TERA project which has received funding from the European Union's Horizon 2020 research and innovation programme under grant agreement NO 824962.

References

[1] R. Drath and A. Horch, "Industrie 4.0: Hit or hype? [industry forum]," *IEEE Industrial Electronics Magazine*, vol. 8, pp. 56–58, June 2014.

[2] C. I, S. Han, Z. Xu, S. Wang, Q. Sun, and Y. Chen, "New paradigm of 5g wireless internet," *IEEE Journal on Selected Areas in Communications*, vol. 34, pp. 474–482, March 2016.

[3] M. Khoshnevisan, V. Joseph, P. Gupta, F. Meshkati, R. Prakash, and P. Tinnakornsrisuphap, "5g industrial networks with comp for urllc and time sensitive network architecture," *IEEE Journal on Selected Areas in Communications*, vol. 37, pp. 947–959, April 2019.

[4] S. A. K. Tanoli, "Utilizing 5g spectrum for healthcare to detect the tremors and breathing activity for multiple sclerosis," *Transactions on Emerging Telecommunications Technologies*, vol. 29, no. 7, pp. e3454–, 2018.

[5] D. Haider, A. Ren, D. Fan, N. Zhao, X. Yang, S. A. Shah, F. Hu, and Q. H. Abbasi, "An efficient monitoring of eclamptic seizures in wireless sensors networks," *Computers & Electrical Engineering*, vol. 75, pp. 16–30, 2019.

[6] H. Korber, H. Wattar, and G. Scholl, "Modular wireless real-time sensor/actuator network for factory automation applications," *IEEE Transactions on Industrial Informatics*, vol. 3, pp. 111–119, May 2007.

[7] K. Islam, W. Shen, and X. Wang, "Wireless sensor network reliability and security in factory automation: A survey," *IEEE Transactions on Systems, Man, and Cybernetics, Part C (Applications and Reviews)*, vol. 42, pp. 1243–1256, Nov 2012.

[8] J. Lee, W. Li, J. Shen, and C. Chuang, "Multi-robotic arms automated production line," in *2018 4th International Conference on Control, Automation and Robotics (ICCAR)*, pp. 26–30, April 2018.

[9] H. G. Jung, Y. H. Cho, P. J. Yoon, and J. Kim, "Scanning laser radar-based target position designation for parking aid system," *IEEE Transactions on Intelligent Transportation Systems*, vol. 9, pp. 406–424, Sep. 2008.

[10] L. Piotrowsky, T. Jaeschke, S. Kuppers, and N. Pohl, "An unambiguous phase-based algorithm for single-digit micron accuracy distance measurements using fmcw radar," in *2019 IEEE MTT-S International Microwave Symposium (IMS)*, pp. 552–555, June 2019.

[11] M. Pauli, B. Gottel, S. Scherr, A. Bhutani, S. Ayhan, W. Winkler, and T. Zwick, "Miniaturized millimeter-wave radar sensor for high-accuracy applications," *IEEE Transactions on Microwave Theory and Techniques*, vol. 65, pp. 1707–1715, May 2017.

[12] S. Scherr, B. Göttel, S. Ayhan, A. Bhutani, M. Pauli, W. Winkler, J. C. Scheytt, and T. Zwick, "Miniaturized 122 ghz ism band fmcw radar with micrometer accuracy," in *2015 European Radar Conference (EuRAD)*, pp. 277–280, Sep. 2015.

[13] S. Ayhan, S. Thomas, N. Kong, S. Scherr, M. Pauli, T. Jaeschke, J. Wulfsberg, N. Pohl, and T. Zwick, "Millimeter-wave radar distance measurements in micro machining," in *2015 IEEE Topical Conference on Wireless Sensors and Sensor Networks (WiSNet)*, pp. 65–68, Jan 2015.

[14] F. Barbon, G. Vinci, S. Lindner, R. Weigel, and A. Koelpin, "A six-port interferometer based micrometer-accuracy displacement and vibration measurement radar," in *2012 IEEE/MTT-S International Microwave Symposium Digest*, pp. 1–3, June 2012.

[15] S. Lindner, F. Barbon, S. Linz, S. Mann, R. Weigel, and A. Koelpin, "Distance measurements based on guided wave 24ghz dual tone six-port radar," in *2014 11th European Radar Conference*, pp. 57–60, Oct 2014.

[16] C. Sturm and W. Wiesbeck, "Waveform design and signal processing aspects for fusion of wireless communications and radar sensing," *Proceedings of the IEEE*, vol. 99, pp. 1236–1259, July 2011.

[17] Q. Wu, F. Zhao, X. Ai, X. Ai, J. Liu, and S. Xiao, "Compressive-sensing-based simultaneous polarimetric hrrp reconstruction with random ofdm pair radar signal," *IEEE Access*, vol. 6, pp. 37837–37849, 2018.

[18] C. Knill, F. Roos, B. Schweizer, D. Schindler, and C. Waldschmidt, "Random multiplexing for an mimo-ofdm radar with compressed sensing-based reconstruction," *IEEE Microwave and Wireless Components Letters*, vol. 29, pp. 300–302, April 2019.

[19] S. Sen and A. Nehorai, "Target detection in clutter using adaptive ofdm radar," *IEEE Signal Processing Letters*, vol. 16, pp. 592–595, July 2009.
[20] S. Sen, "Adaptive ofdm radar waveform design for improved micro-doppler estimation," *IEEE Sensors Journal*, vol. 14, pp. 3548–3556, Oct 2014.
[21] Y. Liu, G. Liao, J. Xu, Z. Yang, and Y. Zhang, "Adaptive ofdm integrated radar and communications waveform design based on information theory," *IEEE Communications Letters*, vol. 21, pp. 2174–2177, Oct 2017.
[22] J. Lim, S. Kim, and D. Shin, "Two-step doppler estimation based on intercarrier interference mitigation for ofdm radar," *IEEE Antennas and Wireless Propagation Letters*, vol. 14, pp. 1726–1729, 2015.
[23] G. Hakobyan and B. Yang, "A novel intercarrier-interference free signal processing scheme for ofdm radar," *IEEE Transactions on Vehicular Technology*, vol. 67, pp. 5158–5167, June 2018.
[24] X. Tian, T. Zhang, Q. Zhang, and Z. Song, "High accuracy doppler processing with low complexity in ofdm-based radcom systems," *IEEE Communications Letters*, vol. 21, pp. 2618–2621, Dec 2017.